Pathophysiology of right ventricular heart disease: the role of structure, apoptosis and inflammation

Campian, M.E.

Publication date
2012

CHAPTER IV

Serial noninvasive assessment of apoptosis during right ventricular disease progression in rat

Maria E. Campian, Hein J. Verberne, Maxim Hardziyenka; Kora de Bruin, Alexander T. Soufan; Mariana Selwanes, Maurice J.B. van den Hoff, Jan M. Ruijter, Berthe L.F. van Eck-Smit, Jacques M.T. de Bakker, Hanno L. Tan

J Nucl Med. 2009 Aug;50(8):1371-7. Epub 2009 Jul 17

"The function of wisdom is to discriminate between good and evil".

George Bernard Shaw

Abstract

Introduction: Right ventricular (RV) function is the major determinant of survival in patients with pulmonary hypertension. Yet, the pathophysiologic basis of RV disease is unresolved. We aimed to study 1) the role of apoptosis in right ventricular (RV) disease by monitoring it serially during disease progression using *in vivo* ^{99m}Tc-Annexin-V (^{99m}Tc-ANX) scintigraphy; 2) whether reduction in apoptosis resulting from chronic treatment with valsartan (VAL) can be detected by ^{99m}Tc-ANX scintigraphy.

Methods: RV disease following pulmonary hypertension was induced by monocrotaline (MCT) injection in rats. Three groups were studied: MCT-treated (MCT-rats), rats treated with MCT+VAL (VAL-rats), and age-matched controls (CON-rats). Serial echocardiography and *in vivo* ^{99m}Tc-ANX scintigraphy were performed. Apoptosis was confirmed by ^{99m}Tc-ANX autoradiography and TUNEL. Fibrosis was assessed by Picro-sirius Red staining.

Results: In MCT-rats, *in vivo* ^{99m}Tc-ANX uptake peaked early and declined thereafter, but remained elevated compared to baseline. These stage-dependent changes of *in vivo* ^{99m}Tc-ANX uptake were paralleled by changes in autoradiography and TUNEL. VAL-rats had longer RV failure-free survival than MCT-rats, along with reduced apoptosis. These changes were accompanied by commensurate delays in RV hypertrophy and RV dilation. VAL-rats also had less fibrosis than MCT-rats at all disease stages.

Conclusion: RV disease progression is associated with an early increase in RV apoptosis, as monitored using serial *in vivo* ^{99m}Tc-ANX scintigraphy. Delay in RV disease progression by VAL is accompanied by reduction in

RV apoptosis. Apoptosis plays a role in RV disease progression and may be assessed by serial *in vivo* ^{99m}Tc-ANX scintigraphy.

Introduction

Right ventricular (RV) disease receives increasing clinical recognition [1]. RV (dys) function is the major determinant of survival in patients with pulmonary hypertension, regardless of the underlying cause [2]. However, the pathophysiologic basis of RV disease is unresolved [3].

The molecular mechanisms that underlie left ventricular (LV) disease progression have been intensely studied [4-6]. It is generally accepted that apoptosis [7] plays an important role in LV disease. Moreover, accumulation of collagen was demonstrated in hypertrophied and failing hearts [8]. Apoptosis and fibrosis have been shown to act in isolation or in concert to reduce LV performance [9,10]. In contrast, the association of apoptosis with RV disease progression [11,12] is unclear. Recently, *in vivo* imaging of cardiac apoptosis with the use of ^{99m}Tc-annexin V (^{99m}Tc-ANX) was proven feasible, as ^{99m}Tc-ANX binds to exposed phosphatidylserine on the outer surface of apoptotic cells [13]. These studies demonstrated apoptosis at single time points. Clearly, serial monitoring of apoptosis *in vivo* is relevant. This may not only provide insight into the time course of apoptosis, but it may also aid in determining the optimal timing of anti-apoptotic therapy, and in assessing the efficacy of therapy. We aimed to study the role of apoptosis in RV disease progression with the use of serial *in vivo* ^{99m}Tc-ANX scintigraphy. Furthermore, we aimed to establish whether reduction in apoptosis resulting from treatment with the angiotensin II receptor-1 blocker (ARB), valsartan (VAL), can be detected *in vivo*. ARBs have been shown to exert beneficial effects on RV disease [14]. These effects may be due to inhibition of apoptosis, as angiotensin II is a mediator of apoptosis [15,16].

Methods

Study design

This investigation was performed in accordance with the *Guide for the Care and Use of Laboratory Animals* published by the US National Institutes of Health (NIH publication 85-23, revised 1996). Male 8-weeks old Wistar rats, weighing 225-285g at the beginning of the experiment, were studied. RV disease was induced with a single intraperitoneal injection (60mg/kg body weight) of monocrotaline (MCT). MCT injection leads to severe pulmonary disease in the absence of intrinsic heart and lung disease [17]. The ensuing pulmonary hypertension results in RV hypertrophy and RV failure. We monitored changes in RV function and apoptosis over time in untreated rats (MCT-rats) and rats that received long-term treatment with VAL (10mg/kg/day, dissolved in saline, kindly provided by Novartis, Switzerland), administered *via* Alzet™ osmotic minipumps that were implanted subcutaneously directly before MCT injection (VAL-rats). As a control group (CON-rats), we used age-matched rats that received intraperitoneal saline with/without VAL *via* osmotic minipumps; we pooled these groups because there were no significant differences between them.

Cardiac function and *in vivo* apoptosis were serially monitored by echocardiography and *in vivo* ^{99m}Tc-ANX scintigraphy, respectively, in 10 rats of each treatment group (CON, MCT, and VAL). Measurements were performed twice a week and the rats were sacrificed after a maximum of 6 weeks or when RV failure occurred. To distinguish whether the *in vivo* ^{99m}Tc-ANX signal originated in RV or LV, we harvested hearts at each of three stages of RV disease progression (RV hypertrophy, RV dilation, and RV failure) and performed *ex vivo* tracer autoradiography in 10 CON-rats and 10 MCT-rats, with n=3 in RV hypertrophy, n=3 in RV dilation, and n=4

in RV failure in each group. In addition, 12 CON-rats, 12 MCT-rats and 12 VAL-rats were sacrificed for TUNEL assays, with n=4 at each RV disease stage. RV hypertrophy and RV dilation were identified using serial echocardiography. RV failure was defined by clinical signs (body weight loss, cyanotic ears, cold limbs, and dyspnea) [18].

Echocardiography

Transthoracic two-dimensional, M-mode and Doppler echocardiography was performed in accordance with the standards of the American Society of Echocardiography, using a 10MHz transducer in anesthetized, spontaneously breathing, rats (3% isoflurane). The dose of the anaesthetic was reduced by 50% in RV failure rats. RV free wall thickness (RVFWT) was measured in the two-dimensional short-axis parasternal view below the tricuspid valve or in the long-axis parasternal view by M-mode, depending on the quality of visualization. RV end-diastolic diameter (RVEDD) was measured as the maximal distance from the RV free wall to the interventricular septum from the apical four-chamber view. Each parameter was averaged over 3 cardiac cycles. RV hypertrophy was defined by RVFWT>0.7mm (22.2±1.7days after MCT injection in MCT-rats), RV dilation by RVEDD>4.5mm (27.0±1.7 days in MCT-rats) [18].

^{99m}Tc-Annexin-V scintigraphy

After the echocardiographic recordings, 40MBq ^{99m}Tc-ANX was injected into a tail vein. Anterior planar scintigraphy was performed one hour thereafter with a dedicated single pinhole system designed for SPECT [19]. Acquisition in the left anterior oblique position was not feasible due to overprojection of nonspecific bone marrow uptake. Rats were immobilized in a perspex cylinder, mounted on a stepping-motor driven system and positioned above the up-facing pinhole collimator of the γ-camera. This

enables anterior scintigraphy at a standardized orientation and distance from the pinhole aperture. In the present study, a tungsten insert with a 3mm pinhole aperture was used. SPECT images could not be reliably reconstructed due to minimal myocardial ^{99m}Tc-ANX uptake. SPECT is therefore not part of the current analysis. The γ-camera was connected to a HERMES acquisition and processing station. Static images of the thorax were obtained for 20min with a 20% energy window at the 140-keV ^{99m}Tc photon peak in a 128x128 matrix. One standardized region of interest (ROI) was drawn over the myocardium (specific activity) and two over extra-thoracic soft tissue in the axilla (nonspecific activity). As there were no differences in the results for the two axillary ROIs, the data were combined to produce aggregate axillary uptake data for further analysis. Myocardial uptake ratio was calculated as the ratio of specific and nonspecific uptake (expressed as mean counts/pixel) as follows: (myocardium-nonspecific)/nonspecific. The image analyzer was blinded to the disease stage of the rats.

Tracer autoradiography

After *in vivo* scintigraphy, the animals were sacrificed and their hearts were used for tracer autoradiography using phosphor imaging. The hearts were excised, quickly frozen and sliced into 50µm short axis slices. Every fifth slice was mounted on a glass plate and covered with a Saran wrap to prevent contamination of the phosphor plate. The short axis slices were exposed to a Fuji BAS-MS imaging plate for ~24h. The images were scanned at 50µm resolution with a 16-bit pixel depth using a Fuji FLA-3000 phosphor imager and analyzed using AIDA image software (Version 3.20.007). For ^{99m}Tc, this technique has a strong linear relation between activity and photo-

stimulated luminescence, and a high resolution of 0.35±0.06mm, expressed as full width half-maximum [20].

TUNEL

In situ terminal deoxynucleotidyl-transferase-mediated dUTP nick-end labeling (TUNEL) was performed using the In Situ Apoptosis Detection Kit POD (Roche, Germany) [21]. Histologic sections were prepared and stained according to the manufacturer's instructions. As a negative control, the TdT enzyme was omitted from the assay. As a positive control, we used rat colon. Methyl-green and hematoxylin-eosin were used as counterstaining for non-cardiomyocytes and colon cell respectively. The number of TUNEL-positive cardiomyocyte nuclei was expressed as percentage of the total number of cardiomyocyte nuclei and was called the apoptosis index. Six paraffin sections (7μm thickness) from each tissue block were obtained at 210μm distances in the coronal plane. In each section, 10 random microscopic fields from RV and LV each were analyzed. Thus, the number of TUNEL-positive cardiomyocytes was determined in 60 microscopic fields (light microscopy, 40 X magnifications) from RV and LV of each animal. We studied 12 rats in each study group, i.e., 4 rats at each of the 3 stages of RV disease progression (RV hypertrophy, RV dilation, and RV failure). The reader was blinded to the disease stage.

Picro-sirius Red staining

To assess the total collagen in myocardial tissue, specimens were stained with Picro-sirius Red F3BA. Tissue sections of 7μm thickness were treated and incubated in 0.1% Picro-sirius Red. Before dehydration, the slides were treated with 0.01N HCL and mounted. Four animals per group were analyzed. Analysis was performed in 60 microscopic fields from RV and LV which was obtained as previously described. The Picro-sirius Red

stained area was expressed as a percentage of the total ventricular tissue area using Image Pro Plus (version 5.02).

Statistical analysis

Two-way analysis of variance (factors treatment and time or disease stage) was performed. Because of a significant interaction between treatment and time, the initial analysis was followed by a one-way analysis between treatments per time point or disease stage. For analysis of the echocardiographic data, these data were fit to an exponential curve (to reflect RV hypertrophy) through the mean values of RVFWT and RVEDD per time point. Delay in time was calculated as the average time distance between these best fitted exponential curves, including all data points for which the treated groups had RVFWT and RVEDD above control values. Data are expressed as mean±SEM. *P value* of less than 0.05 was considered to indicate a statistically significant difference.

Results

Apoptosis detection during the natural time course of RV disease progression

- *Serial in vivo ^{99m}Tc-ANX scintigraphy*

Figure 1A shows ^{99m}Tc-ANX uptake in a MCT-rat in the RV hypertrophy stage (right) and an age-matched CON-rat (left). MCT-rats exhibited a biphasic time course of ^{99m}Tc-ANX uptake (Figure 1B, squares). Initially, ^{99m}Tc-ANX uptake increased and became significantly higher than baseline at 15 days after MCT injection. Thereafter, ^{99m}Tc-ANX uptake declined towards the end of the study (RV failure), but remained elevated compared to baseline. ^{99m}Tc-ANX uptake remained at baseline levels in CON-rats (Figure 1B, triangles).

Figura 1

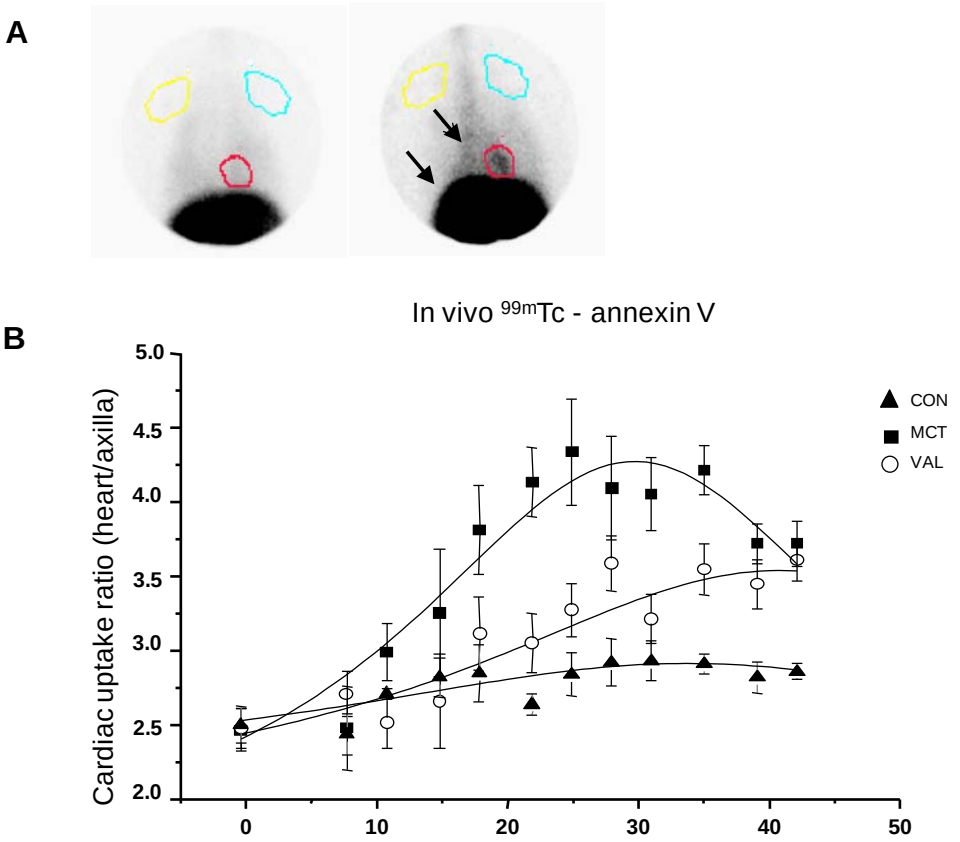

In vivo detection of apoptosis using ^{99m}Tc-annexin-V scintigraphy. A. Representative planar pinhole scintigrams 1 hour after intravenous injection of ^{99m}Tc-annexin-V in a MCT-rat in the RV hypertrophy stage (right panel) and age-matched CON-rat (left panel). Regions of interest were drawn around the myocardium (red) and in the extra-thoracic soft tissue (yellow, blue) to determine the cardiac uptake ratio. Note ^{99m}Tc-annexin-V uptake in the cardiac region and liver (arrow) of the MCT-rat. **B.** Cardiac uptake ratios at various times after MCT injection, n=10 per group. $p<0.05$ from day 15 until day 42 in MCT-rats (square) and from day 18 until day 42 in VAL-rats (circles) vs. age-matched CON-rats (triangle). CON, age-matched control; MCT, monocrotaline-injected rat; VAL, valsartan-treated rat; RV, right ventricle. Data are mean±SEM.

- *Ex vivo quantitative ^{99m}Tc-ANX autoradiography*

Planar *in vivo* ^{99m}Tc-ANX scintigraphy did not allow us to distinguish whether the observed ^{99m}Tc-ANX uptake occurred in RV or LV. To resolve this issue, we conducted *ex vivo* semi-quantitative ^{99m}Tc-ANX

autoradiography. Because the time course of *in vivo* ^{99m}Tc-ANX uptake suggested differential ^{99m}Tc-ANX uptake at the three successive RV disease stages, rats were sacrificed at each stage. We found increased ^{99m}Tc-ANX uptake in RV at all stages in MCT-rats compared to CON-rats. This signal was highest at the RV hypertrophy stage (Figure 2). In contrast, the autoradiography signal in LV did not change between disease stages in CON-rats and MCT-rats.

Figure 2

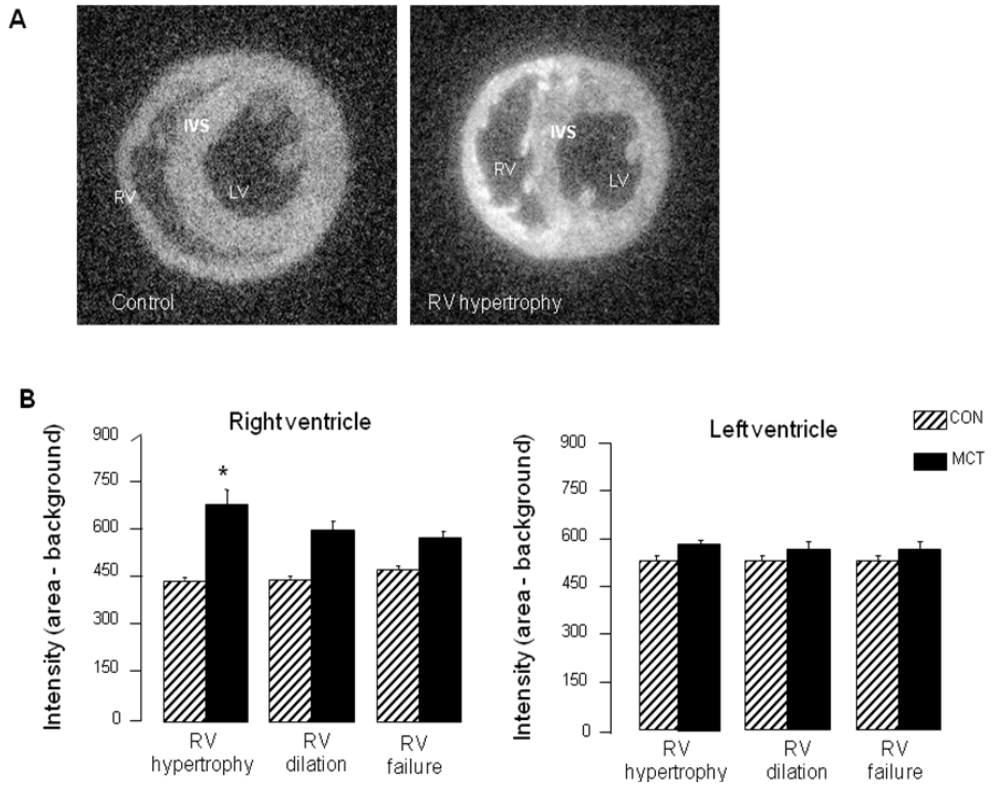

^{99m}Tc-ANX autoradiography. A. Representative short axis myocardial slices from a MCT-rat in the RV hypertrophy stage (right) and an age-matched CON-rat (left). Note higher signal intensity in RV compared to the interventricular septum (IVS) or LV (background). **B.** Signal intensities of region of interest minus background (PSL/mm2), n=10 in CON and MCT groups each, with n=3 at RV hypertrophy and RV dilation, and n=4 in RV failure. *p<0.05 vs. age-matched CON-rat. PSL: photo-stimulated luminescence, other abbreviations as in Figure 1. Data are mean±SEM.

- *TUNEL analysis*

Figure 3

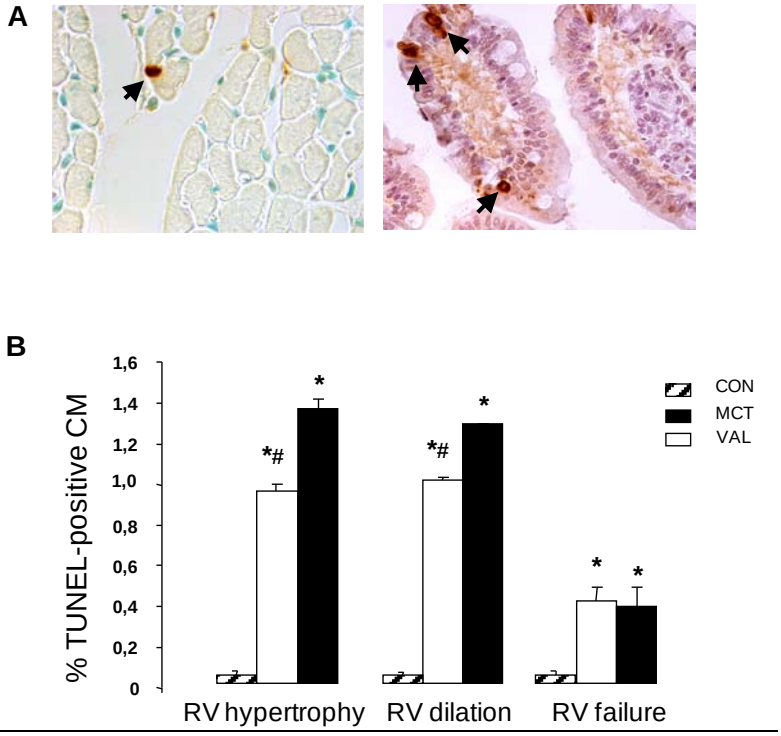

TUNEL staining. A. Representative examples of apoptotic cell. Left panel: TUNEL-positive cardiomyocyte (arrow), methyl green counterstain. Right panel: positive control, TUNEL-positive rat colon cell (arrows). **B.** Apoptosis index during RV disease progression, n=4 per disease stage in each group. *p<0.001 vs. CON-rat; #p<0.01 vs. MCT-rat. Abbreviations as in Figure 2. Data are mean±SEM.

To obtain histologic confirmation that ^{99m}Tc-ANX uptake reflected apoptosis, we determined the apoptosis index using TUNEL assays of RV and LV. Figure 3A shows a TUNEL-positive cardiomyocyte (arrow left panel) in a MCT-rat heart and a TUNEL-positive rat intestine cell (positive control, arrow right panel). The stage-dependent changes in apoptosis index of MCT-rats paralleled those of the ^{99m}Tc-ANX autoradiography signal, while the apoptosis index of CON-rats remained at baseline levels. Thus, the apoptosis index of MCT-rats was increased over age-matched CON-rats at

all three stages and highest during RV hypertrophy. In LV, TUNEL-positive cardiomyocytes were virtually undetectable at all disease stages (data not shown).

Taken together, these findings indicate that serial ^{99m}Tc-ANX scintigraphy allows for noninvasive evaluation of the time course of RV apoptosis. To establish whether ^{99m}Tc-ANX scintigraphy may also be used to monitor the effects of therapies that counteract RV disease progression by reducing RV apoptosis, we next conducted ^{99m}Tc-ANX scintigraphy in VAL-rats.

Apoptosis detection during long-term valsartan treatment

- *Serial echocardiographic measurements of RV function*

The onsets of RV hypertrophy and RV dilation, as assessed by echocardiography, were delayed by 5.5±0.3days and 4.4±0.3days, respectively, in VAL-rats compared to MCT-rats (Figure 4 A and 4 B).

Figure 4

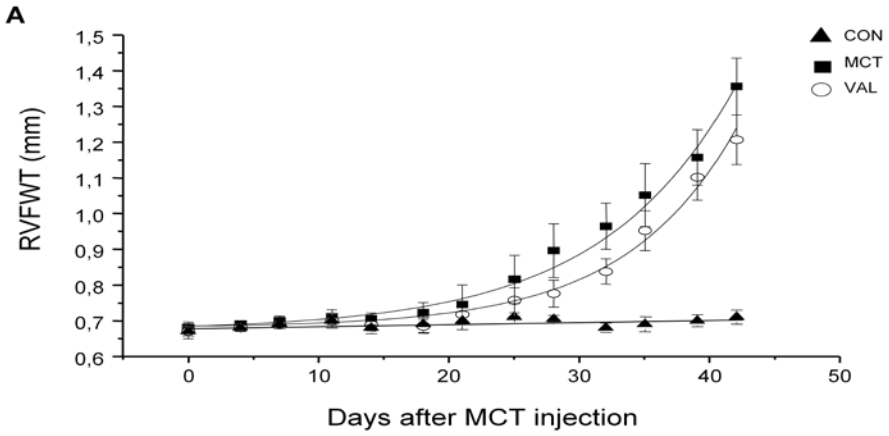

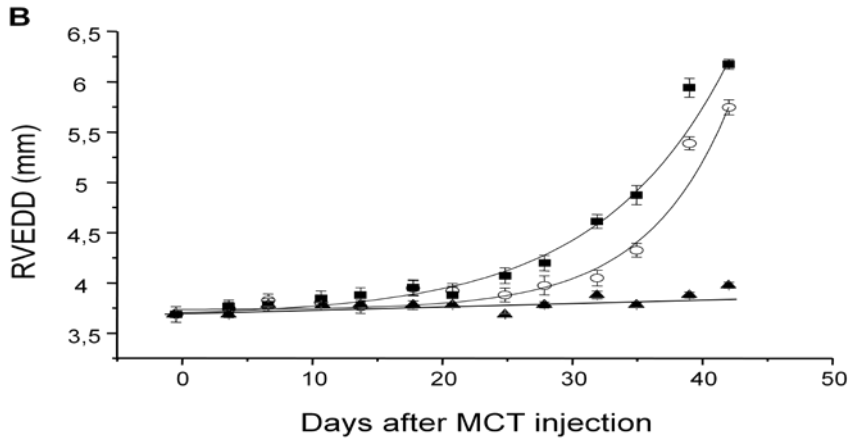

Time course of development of RV hypertrophy and RV dilation. A. Time course of development of RV hypertrophy assessed echocardiographically by RV free wall thickness (RVFWT). **B.** Time course of development of RV dilation assessed echocardiographically by RV end-diastolic diameter (RVEDD). Abbreviations as in Figure 2. Data are mean±SEM.

- *In vivo ^{99m}Tc-ANX uptake*

In accordance with the delay in the onset of the successive RV disease stages in VAL-rats, the increase of *in vivo* ^{99m}Tc-ANX uptake of these rats was delayed, as ^{99m}Tc-ANX uptake became significantly higher than baseline only at 18 days after MCT injection (Figure 1B, circles). Moreover, the ^{99m}Tc-ANX uptake was lower in VAL-rats than in MCT-rats throughout disease progression. Still, the ^{99m}Tc-ANX uptake of VAL-rats was significantly increased over CON-rats at day 42 after MCT injection.

- *TUNEL*

The apoptosis index in VAL-rats exhibited the same time course as in MCT-rats (Figure 3), but it was significantly lower in VAL-rats than in MCT-rats at the RV hypertrophy and RV dilation stages.

Collagen deposition

MCT-rats exhibited increased levels of interstitial collagen deposition. In contrast to the changes in RV apoptosis which peaked at early RV disease

stages, the amount of RV fibrosis continuously increased throughout RV disease progression, being highest during RV failure (Figure 5A). In LV, collagen levels remained at baseline (not shown). VAL-rats had a similar time course of RV fibrosis as MCT-rats, but RV fibrosis levels were significantly lower than in MCT-rats at all disease stages (Figure 5B). LV fibrosis remained unaltered, similar to MCT-rats (not shown).

Figure 5

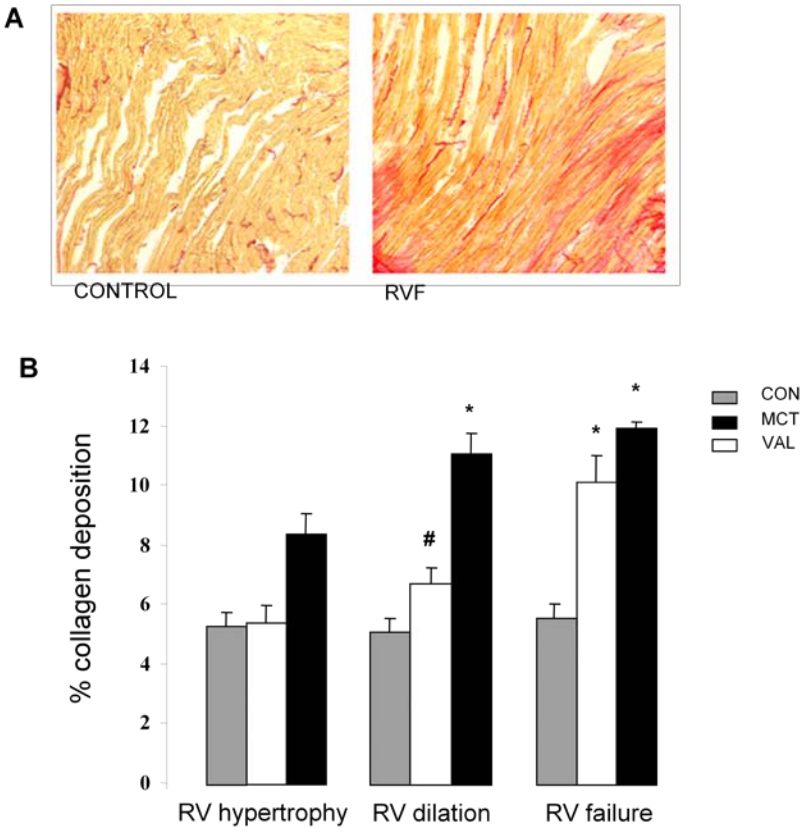

Collagen deposition. A. Representative sections of interstitial fibrosis using Picro-sirius Red staining from a CON-rat (left panel) and a MCT-rat with RV failure (right panel). Note homogenous distribution of Picro-sirius Red staining in RV during RV failure. **B.** Quantification of collagen deposition during RV disease progression, n=4 per group; *p<0.01 vs. age-matched controls. Abbreviations as in Figure 2. Data are mean±SEM.

Discussion

We found increases in apoptosis during early stages of RV disease progression that can be monitored by serial *in vivo* ^{99m}Tc-ANX scintigraphy. Moreover, delay in RV disease progression by VAL treatment paralleled reduction in RV apoptosis, as detected using *in vivo* ^{99m}Tc-ANX scintigraphy. These findings demonstrate that noninvasive serial monitoring of myocardial apoptosis during RV disease progression is feasible and has potential clinical relevance.

We demonstrate that serial ^{99m}Tc-ANX scintigraphy can be used to monitor RV apoptosis throughout disease progression in a noninvasive manner. The ^{99m}Tc-ANX scintigram signal reflected apoptosis, as confirmed by ^{99m}Tc-ANX autoradiography and TUNEL, and exhibited a particular time course, peaking at early disease stages (hypertrophy) and declining thereafter (failure), but remaining significantly increased over baseline values at all RV disease stages. Furthermore, we found that a delay in RV disease progression by VAL was attended by a reduction in RV apoptosis, as detected with serial *in vivo* ^{99m}Tc-ANX scintigraphy. This observation not only illustrates that serial *in vivo* ^{99m}Tc-ANX scintigraphy may be used to monitor the effects of therapy aimed at counteracting apoptosis, but supports the notion that apoptosis is causally related to RV disease in this model. Still, it must be noted that it does not prove a causal relation, because RV disease progression was not completely arrested, and apoptosis was not completely abolished.

^{99m}Tc-ANX scintigraphy has been effectively used to noninvasively map regions of apoptosis in patients with various pathologies [22-26], as well as in experimental model of autoimmune myocarditis [27]. We anticipate that the ability to detect apoptosis serially *in vivo* using ^{99m}Tc-

ANX scintigraphy, as demonstrated in the present study, will not only facilitate mechanistic studies related to apoptosis, but will also allow for monitoring of the disease course or the response to various treatments aimed at counteracting RV failure. Using serial echocardiography allowed us to pinpoint apoptosis to specific RV disease stages. Defining the disease stages precisely is of great value to conduct such studies. The occurrence of apoptosis during early RV disease stages suggests a potentially beneficial effect of apoptosis inhibition. We found that apoptosis started early and declined when clinically manifest RV failure occurred. This finding is consistent with other pressure-overload mediated RV disease studies [11,12].

Our findings that VAL administration delayed RV disease progression correspond to the reported protective effects of olmesartan in the same animal model [14]. Yet, they contrast with studies which showed that losartan did not prevent RV hypertrophy in the MCT model [28,29]. These discrepancies may be due to greater potency of newer ARBs (VAL, olmesartan) over first-generation ARBs (losartan). Furthermore, our results are consistent with the Valsartan Heart Failure Trial which showed that VAL attenuates morbidity in LV failure patients [30,31].

Chronic activation of the RAAS plays an important role in the structural and functional pathogeneses of heart failure. AII provides the pathophisiological insight in the development of cardiac fibrosis and heart failure. Moreover, it is now generally accepted that apoptosis is mediated via type-1 angiotensin II receptors (AT1) [15,16]. Leri et al. [32] and Li et al [33] demonstrated *in vitro* that myocyte stretch-induced apoptosis can be inhibited by losartan.

Our study shows that delay in RV disease progression is not only associated with a reduction in apoptosis, but also with reduced collagen deposition. The mechanisms leading to angiotensin II induced fibrosis are thought to be at least in part mediated through growth factor pathways induced by AT1 activation [34,35].

Although our findings are in line with previous studies in LV disease which provided clear evidence that apoptosis promotes heart failure, estimates regarding the amount of cell death from apoptosis, and the role of apoptosis in the progression into heart failure, are still controversial. The reported percentage of apoptosis in end-stage LV failure is similar to our findings in the RV failure stage [36]. However, the contribution of apoptosis to disease progression remains controversial. Studies from a transgenic mouse model of cardiac-restricted expression of ligand-activated pro-caspase 8 have demonstrated that even low levels of cardiomyocyte apoptosis are sufficient to cause lethal dilated cardiomyopathy [37]. Furthermore, in end-stage LV failure, oncosis and autophagic cell death have also been reported to play an important role in disease progression [38]. The role of these alternative modes of cell death in RV disease progression remains to be explored.

Our study has several limitations. Recent studies have shown that phosphatidylserine externalization occurs not only in apoptosis but also in activated macrophages. Furthermore, it has been shown that annexin binds to externalized phosphatidylserine and can also be internalized through an annexin-specific mechanism. These findings suggest that annexin cannot exclusively be used as a marker of apoptosis but can also be used to visualize inflammation [39]. We did not conduct double staining to exclude the possibility that ^{99m}Tc-annexin V was bound by non-cardiomyocytes.

Still, we found that all apoptosis assays which we used (^{99m}Tc-ANX scintigraphy and autoradiography, and TUNEL staining) were consistent with each other, exhibiting similar time-dependent changes throughout RV disease progression. These findings suggest that these signals faithfully reflected the time course of apoptosis during RV disease throughout the time course of apoptosis, which we believe is strongly associated with apoptotic cardiomyocytes in our animal model.

Conclusions

In vivo ^{99m}Tc-ANX scintigraphy may be used for the serial assessment of apoptosis throughout RV disease progression, and the efficacy of treatments aimed at counteracting apoptosis. Thus, *in vivo* ^{99m}Tc-ANX scintigraphy is a valuable tool for mechanistic studies, drug development and clinical management alike, because of its easy implementation and its noninvasive nature.

Acknowledgments

We are grateful to Dr. Alexandre T. Soufan for his expertise in developing the software analysis.

This work was supported in part by the Royal Netherlands Academy of Arts and Sciences (KNAW) and Netherlands Organization for Scientific Research (NWO, ZonMW VICI 918.86.616).

References

1. Hadda F, Doyle R, Murphy DJ, Hunt SA. Right ventricular function in cardiovascular disease, part II: pathophysiology, clinical importance, and management of right ventricular failure. *Circulation 2008;117:1717-31*.
2. Voelkel NF, Quaife RA, Leinwand LA, et al. Right ventricular function and failure: report of a National Heart, Lung, and Blood Institute working group on cellular and molecular mechanisms of right heart failure. *Circulation 2006;114:1883-91*.
3. Bleasdale RA, Frenneaux MP. Prognostic importance of right ventricular dysfunction. *Heart 2002;88:323-4*.
4. Abbate A, Scarpa S, Santini D, et al. Myocardial expression of survivin, an apoptosis inhibitor, in aging and heart failure: an experimental study in the spontaneously hypertensive rat. *Int J Cardiol 2005;111:371-6*.
5. Feldman AM, Weinberg EO, Ray PE, Lorell BH. Selective changes in cardiac gene expression during compensated hypertrophy and the transition to cardiac decompensation in rats with chronic aortic banding. *Circ Res 1993;73:184-92*.
6. Berenji K, Drazner MH, Rothermel A, Hill JA. Does load-induced ventricular hypertrophy progress to systolic heart failure? *Am J Physiol 2005;289:H8-H16*.
7. Anversa PL, Leri A, Beltrami CA, Guerra S, Kajstura J. Myocyte death and growth in the failing heart. *Lab Invest 1998;78:767-86*.
8. Weber KT. Targeting pathophysiological remodeling: concepts of cardioprotection and reparation. *Circulation 2000;102:1342-45*.
9. Sabbah HN, Stein PD, Kono T, et al. A canine model of chronic heart failure produced by multiple sequential coronary microembolizations. *Am J Physiol 1991;260:H1379-84*.
10. Schaper J, Froede R, Hein S, et al. Impairment of the myocardial ultrastructure and changes of the cytoskeleton in dilated cardiomyopathy. *Circulation 1991;83:504-14*.
11. Ecarnot-Laubriet A, Assem M, Poirson-Bichat F, et al. Stage-dependent activation of cell cycle and apoptosis mechanisms in the right ventricle by pressure overload. *Biochim Biophys Acta 2002;1586:233-42*.
12. Ikeda S, Hamada M, Hiwada K. Cardiomyocyte apoptosis with enhanced expression of P53 and Bax in right ventricle after pulmonary arterial banding. *Life Sci 1999;65:925-33*.
13. Blankenberg FG, Katsikis PD, Tait JF, et al. In vivo detection and imaging of phosphatidylserine expression during programmed cell death. *PNAS 1998;95:6349-54*.
14. Kato T, Nasu T, Sonoda H, Ito KM, Ikeda M, Ito K. Evaluation of olmesartan medoxomil in the rat monocrotaline model of pulmonary hypertension. *J Cardiovasc Pharmacol 2008;51:18-23.*

15. Cigola E, Kajstura J, Li B, Meggs LG, Anversa P. Angiotensin II activates programmed myocyte cell death in vitro. *Exp Cell Res 1997;231:363-71*.
16. Li D, Tomson K, Yang B, Mehta P, Croker BP, Mehta JL. Modulation of constitutive nitric oxide synthase, bcl-2 and Fas expression in cultured human coronary endothelial cells exposed to anoxia-reoxygenation and angiotensin II: role of AT1 receptor activation. *Cardiovasc Res 1999;41:109-15*.
17. Lalich JJ, Merkow L Pulmonary arteritis produced in rats by feeding. Crotolaria spectabilis. *Lab Invest 1961;10:744-50*.
18. Hardziyenka M, Campian ME, de Bruin-Bon RHACM, Michel MC, Tan HL Sequence of echocardiographic changes during development of right ventricular failure in rat. *J Am Soc Echocardiogr 2006;19:1272-9*.
19. Habraken JBA, de Bruin K, Shehata M, Booij J, et al. Evaluation of high-resolution pinhole SPECT using a small rotating animal. *J Nucl Med 2001;42:1863-9*.
20. Knol RJJ, de Bruin K de Jong J, van Eck-Smit BLF, Booij J. In vitro and ex vivo storage phosphor imaging of short-living radioisotopes. *J Neurosci Meth 2008;168:341-57*.
21. Gavrieli Y, Sherman Y, Ben-Sasson SA. Identification of programmed cell death in situ via specific labeling of nuclear DNA fragmentation. *J Cell Biol 1992;119:493-501*.
22. Hofstra L, Liem IH, Dumont EA, et al. Visualisation of cell death in vivo in patients with acute myocardial infarction. *Lancet 2000;356:209-12*.
23. Vriens P, Blankenberg F, Stoot J, et al. The use of technetium Tc 99m annexin V for in vivo imaging of apoptosis during cardiac allograft rejection. *J Thorac Cardiovasc Surg 1998;11:844-53*.
24. Hofstra L, Dumont EA, Thimister PW, et al. In vivo detection of apoptosis in an intracardiac tumor. *JAMA 2001;285:1841-2*.
25. Kietselaer BL, Reutelingsperger CP, Boersma HH, et al. Noninvasive detection of programmed cell loss with 99mTc-labeled annexin A5 in heart failure. *J Nucl Med 2007;48:562-7*.
26. Narula J, Strauss HW. P.S.* I love you: implications of phosphatidyl serine (PS) reversal in acute ischemic syndromes. *J Nucl Med 2003;44:397-9.*
27. Tokita N, Hasegawa S, Maruyama K, et al. 99mTc-Hynic-annexin V imaging to evaluate inflammation and apoptosis in rats with autoimmune myocarditis. *Eur J Nucl Med Mol Imaging 2003;30:232-8*.
28. Cassis LA, Rippetoe PE, Soltis EE, Painter Dj, Fitz R, Gillespie MN Angiotensin II and monocrotaline-induced pulmonary hypertension: effect of losartan (DuP 753), a nonpeptide angiotensin type 1 receptor antagonist. *J Pharmacol Exp Ther 1992;262:1168-72*.
29. Kreutz R, Fernandez-Alfonso MS, Ganten D, Paul M. Effect of losartan on right ventricular hypertrophy and cardiac angiotensin I-converting enzyme activity in pulmonary hypertensive rats. *Clin Exp Hypertens 1996;18:101-11*.

30. Cohn JN, Tagnoni G Valsartan Heart failure Trial Investigators. A randomized trial of the angiotensin-receptor blocker valsartan in chronic heart failure. *N Eng J Med 2001;345:1667-75*.
31. Krum H, Casson P, Farsang C, et al. Effect of valsartan added to background ACE inhibitor therapy in patients with heart failure: results from Val-HeFT. *Eur J Heart Fail 2004;6:937-45.*
32. Leri A, Liu Y, Claudio PP, et al. Insulin-Like Growth Factor-1 Induces Mdm2 and Down-Regulates p53, Attenuating the Myocyte Renin-Angiotensin System and Stretch-Mediated Apoptosis. *Am J Pathol 1999;154:567-80.*
33. Li D, Yang B, Phillip MI, Metha JL Proapoptotic effects of ANG II in human coronary artery endothelial cells: role of AT1 receptor and PKC activation. *Am J Physiol 1999;276:H786–92.*
34. Pinto YM, Pinto-Sietsma EJ, Phillip T, et al. Reduction in left ventricular messenger RNA for transforming growth factor beta(1) attenuates left ventricular fibrosis and improves survival without lowering blood pressure in the hypertensive TGR(mRen2)27 Rat. *Hypertension 2000;36:747-54.*
35. Sun Y, Ramires FJ, Zhou G, Ganjam VK, Weber KT. Fibrous tissue and angiotensin II. *J Mol Cell Cadiol 1997;29:2001-12.*
36. Olivetti G, Abbi R, Quaini F, et al. Apoptosis in the failing heart. *N Engl J Med 1997;336:1131-41*.
37. Wencker D, Chandra M, Nguyen K, et al. A mechanistic role for cardiac myocyte apoptosis in heart failure. *J Clin Invest 2003;111:1497-504.*
38. Kostin S, Pool L, Elsässer A, et al. Myocytes die by multiple mechanisms in failing human hearts. *Circ Res 2003;92:715-24.*
39. Laufer EM, Reutelingsperger CPM, Narula J, Hofstra L. Annexin A5: an imaging biomarker of cardiovascular risk. *Basic Res Cardiol 2008; 103: 95-104)*